

pubs.acs.org/JPCL Letter

# Generating Shear Flows without Moving Parts by Thermo-osmosis in Heterogeneous Nanochannels

Xin Wang, Maochang Liu, Dengwei Jing, and Oleg Prezhdo\*



Cite This: J. Phys. Chem. Lett. 2021, 12, 10099-10105



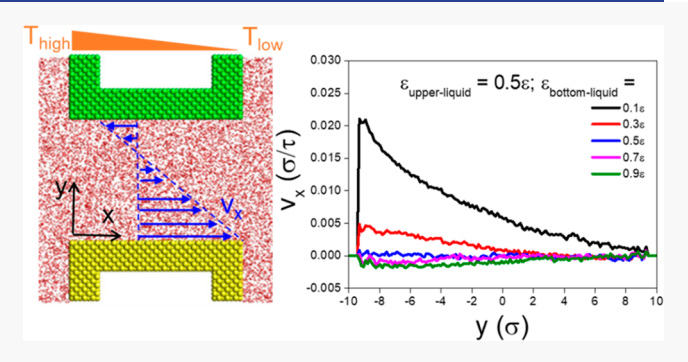
**ACCESS** 

Metrics & More

Article Recommendations

Supporting Information

ABSTRACT: Shear flows play critical roles in biological systems and technological applications and are achieved experimentally using moving parts. However, when the system size is reduced to micro- and nanoscale, fabrication of moving parts becomes exceedingly challenging. We demonstrate that a heterogeneous nanochannel composed of two parallel walls with different wetting behaviors can generate shear flow without moving parts. Molecular dynamics simulations show that shear flows can be formed inside such a nanochannel under a temperature gradient. The physical origin is that thermo-osmosis velocities with different rates and directions can be tuned by wetting behaviors. Our analysis reveals that thermo-osmosis is governed by surface excess enthalpy and



nanoscale interfacial hydrodynamics. This finding provides an efficient method of generating controllable shear flows at micro- and nanoscale confinement. It also demonstrates the feasibility of using fluids to drive micromechanical elements via shear torques generated by harvesting energy from temperature differences.

Shear flows have been found to play critical roles in many areas, from biological systems to various technological applications. To cite a few examples, mammalian sperm cells swimming against environment flows and navigation toward the egg cell have been verified to be controlled by shear flows from experimental and numerical methods. This property is labeled as rheotaxis, which was also reported for other cells. Shear flows can be an efficient method of controlling the dynamics and deformation behaviors of flexible fibers, nanoparticles, and self-propelled colloids. This is important in numerous applications, such as drug delivery, biomolecule separation, and material synthesis, delivery, biomonal scuring, water collection, supercapacitors, sensors and actuators, 22,23 etc. There are also applications in physical sciences, e.g., the thermal conductivity of nanofluids can be enhanced by shear flows, the supercapacitor of the sentence of the supercapacitors of the sentence of the supercapacitors.

Recently, multiple research efforts have been dedicated to investigation of the behavior of fibers in micro- and nanoscale confined situations because of the development of micro- and nanofluidic fluid control technology. These results showed, when the fiber lengths became comparable to the channel dimensions, the interaction of fibers with bounding walls would lead to rich transport dynamics, e.g., snake motions in a shear flow, transportation at zero force in a plug flow, and periodic oscillations between walls. These finding indicate that the coupling between confined walls and background flows could provide a promising approach for accurate control of flexible fibers.

Experimentally, there are two main methods of realizing shear flows. 4,25,31,32 The most common method involves moving parts. The fluids are typically driven by two moving parts with a relative velocity, such as two parallel nested cylinders with different diameters located at the same center shaft, and thus a linear shear flow is distributed between the cylinders. The other method is to use a parabolic velocity distribution characteristic of the Poiseuille flow in the channels. 4,32 An object can experience an approximated shear flow near the walls if the channel height is much larger than the object size.

However, these two methods become cumbersome when the system size is reduced to micro- and nanoscale, in particular because fabrication of moving parts at micro- and nanoscale is still very challenging. Further, rich functions and phenomena can be achieved by tuning wall surface properties, e.g., surface shapes, <sup>33,34</sup> surface energies, <sup>35,36</sup> and surface charges, <sup>37,38</sup> without introducing any moving parts. A fixed structure at micro- and nanoscale is preferred. A typical example among these works is the fluid diode which allows a unidirectional fluid flow. At macro-scale, this function can be

Received: August 25, 2021 Accepted: October 7, 2021 Published: October 11, 2021





achieved by a moving valve. However, at microscale, microvalves containing moving parts would cause reliability issues and require external actuations to provide driving forces. To solve this problem, Li et al. fabricated a moving part-free nanofluidic diode by using nanochannels with heterogeneous surface energies, one-half of which is hydrophilic and the other half is hydrophobic. Picallo et al. suggested that a nanofluidic diode could be built by tuning the asymmetrical surface charges of a nanochannel.

As discussed above, the combination of shear flows and micro- and nanoconfinement is expected to provide promising control of cells, flexible fibers, colloids, etc. However, an efficient method of generating shear flows at micro- and nanoconfinement is still lacking because of the moving parts. To solve this problem, we propose a moving part-free approach to achieving controllable shear flows using a heterogeneous nanochannel. In our design, the upper part of a nanochannel has a moderate wetting behavior while the wetting of the bottom part is varied from very hydrophobic ( $\theta \approx 0^{\circ}$ ) to very hydrophilic ( $\theta \approx 180^{\circ}$ ). The wetting behavior is characterized by the contact angle  $\theta$ , as we will discuss hereafter. As a result, once a temperature gradient is imposed along the nanochannel, different rates and directions of shear flows are formed inside it.

To demonstrate the feasibility of our design, a molecular simulation system consisting of a heterogeneous nanochannel connected by two fluid reservoirs has been constructed, as illustrated in Figure 1. Periodic boundary conditions are

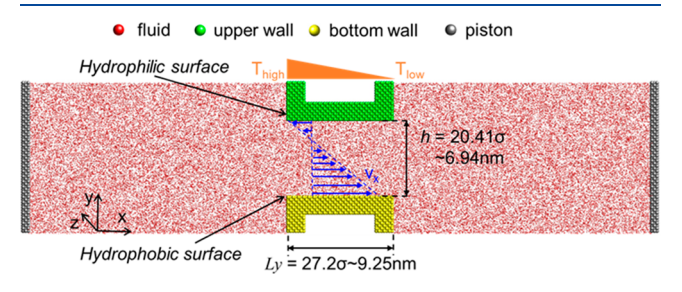


**Figure 1.** Snapshot of the molecular dynamics simulation system. The height and length of nanochannel are labeled as *h* and *Ly*, respectively.

imposed in all directions. Two separated fluid reservoirs are constructed by the pistons and side walls of the nanochannel, and an external force acts on each piston to maintain the reservoir pressure at  $0.1\varepsilon/\sigma^3$ . Two parallel walls are used to form the nanochannel. The size of each wall is  $27.20 \times 4.08 \times 21.77 \ \sigma^3$ . To avoid possible interactions between the nanochannel and its periodic images, side walls are built at the end of the nanochannel. The size of each side wall is  $5.44 \times 4.08 \times 21.77 \ \sigma^3$ . The height of the nanochannel is  $20.41\sigma$ . The initial size of each reservoir is  $68.05 \times 19.73 \times 21.77 \ \sigma^3$ . The size of the simulation box is  $326.62 \times 19.73 \times 21.77 \ \sigma^3$ , which is sufficiently large in the *x*-direction to prevent possible interactions induced by periodic boundary conditions.

The fluids and solids, including walls and pistons, interact with each other through Lennard-Jones (LJ) potentials

$$V(r) = 4\varepsilon \left[ \left( \frac{\sigma}{r} \right)^{12} - \left( \frac{\sigma}{r} \right)^{6} \right]$$
 (1)

where r is the distance between particles and  $\varepsilon$  and  $\sigma$  are energy and length parameters, respectively. The cutoff distance of 4.5 $\sigma$  is chosen. All length parameters  $\sigma$  are set as 1.0 $\sigma$ . For

energy parameters  $\varepsilon$ ,  $\varepsilon_{\rm fluid-fluid} = \varepsilon_{\rm wall-wall} = \varepsilon_{\rm piston-piston} = 1.0\varepsilon$ . To reduce the effect of pistons on fluids,  $\varepsilon_{\rm piston-fluid}$  is set as 0.1 $\varepsilon$ . Different wetting behaviors can be achieved by tuning the values of  $\varepsilon_{\rm wall-fluid}$ , as will be explained later. To prevent melting of the solids and the pistons, a spring force is applied to each solid and piston particle to tether it to its lattice position. The spring constant K is  $2500\varepsilon/\sigma^2$ . LJ reduced units are based on the parameters of the fluid particles: length  $\sigma$ , energy  $\varepsilon$ , and mass m.

All the molecular dynamics simulations have been performed with the LAMMPS package.<sup>41</sup> The time step is  $0.005\tau$ , and the Nose-Hoover thermostat has been used for the NVT ensemble. 70 000 fluid particles are randomly placed in the nanochannel and two reservoirs. The system is first run under the NVT ensemble at  $0.85\varepsilon/k_{\rm b}$  for 100 000 time steps to reach the state of thermal equilibrium. Then, the left and right reservoirs are run under separate NVT ensembles at  $T_{high}$  =  $0.95\varepsilon/k_{\rm b}$  and  $T_{\rm low} = 0.75\varepsilon/k_{\rm b}$ , respectively, for 100 000 time steps to reach stable temperature distributions. The middle parts including the nanochannel and the fluids inside the nanochannel are run under the NVE ensemble to guarantee that they experience no thermostatting. This is used to produce a temperature gradient along the nanochannel. Subsequently, the pistons are allowed to move freely just along the x-direction for 100 000 time steps to reach stable pressure and flow conditions. Finally, an additional 1 000 000 time steps are continued to collect the needed data. For each case, eight independent simulations with different initial velocities and positions of fluid particles are employed to reduce statistical uncertainties.

To construct a heterogeneous nanochannel, the interaction energy between the upper wall of the nanochannel and fluids,  $\varepsilon_{\rm upper-fluid}$ , is set at  $0.5\varepsilon$ . To achieve moderate wetting behavior, the interaction energy between the bottom wall and fluids,  $\varepsilon_{\rm bottom-fluid}$ , is varied from  $0.1\varepsilon$  (very hydrophobic, contact angle  $\theta$  is nearly  $180^{\circ}$ ) to  $0.9\varepsilon$  (very hydrophilic,  $\theta\approx0^{\circ}$ ). The contact angles are  $115^{\circ}$ ,  $62^{\circ}$ , and  $14^{\circ}$  for  $\varepsilon_{\rm bottom-fluid}=0.3,\,0.5,\,$  and  $0.7\varepsilon$ , respectively. We have confirmed this wetting behavior with the same particles of the wall and the fluid by evaluating the contact angle of a droplet put on a wall in our previous work.  $^{42}$ 

We first investigate the velocity distribution inside the nanochannel. Figure 2a shows the velocity field inside the nanochannel in the x-y plane for  $\varepsilon_{\text{upper-fluid}} = 0.5\varepsilon$  and  $\varepsilon_{\rm bottom-fluid} = 0.1\varepsilon$ . The fluid velocity near the bottom very hydrophobic surface points to the lower temperature region and is much larger than the velocity near the upper surface with moderate wetting behavior. Figure 2b shows velocity profiles in the flow direction for varied values of  $\varepsilon_{\rm bottom\text{-}fluid}$  and a fixed value of  $\varepsilon_{\text{upper-fluid}} = 0.5\varepsilon$ . In all figures, y is the distance to the surface, y = 0 is the center of the nanochannel, and y = $\pm 10\sigma$  around the position of the wall surfaces. It is seen that shear flows are formed in the heterogeneous nanochannel with different wetting behaviors under a temperature gradient. The velocity profiles in the middle part of the nanochannel are linear fitted to quantitatively estimate the shear flows. The results as presented in Figure 2c. As seen, the rates and direction of shear flows can be controlled by tuning the surface energy heterogeneity. Especially, much larger shear flows can be achieved by using the hydrophobic surface. Using typical molecular length and energy ( $\sigma = 0.34$  nm and  $\varepsilon = 996.65$ J/ mol) and time ( $\tau = 1$  ps), the maximum value of shear flows under a temperature gradient ~2.7 K/nm is on the order of  $|\gamma|$ 

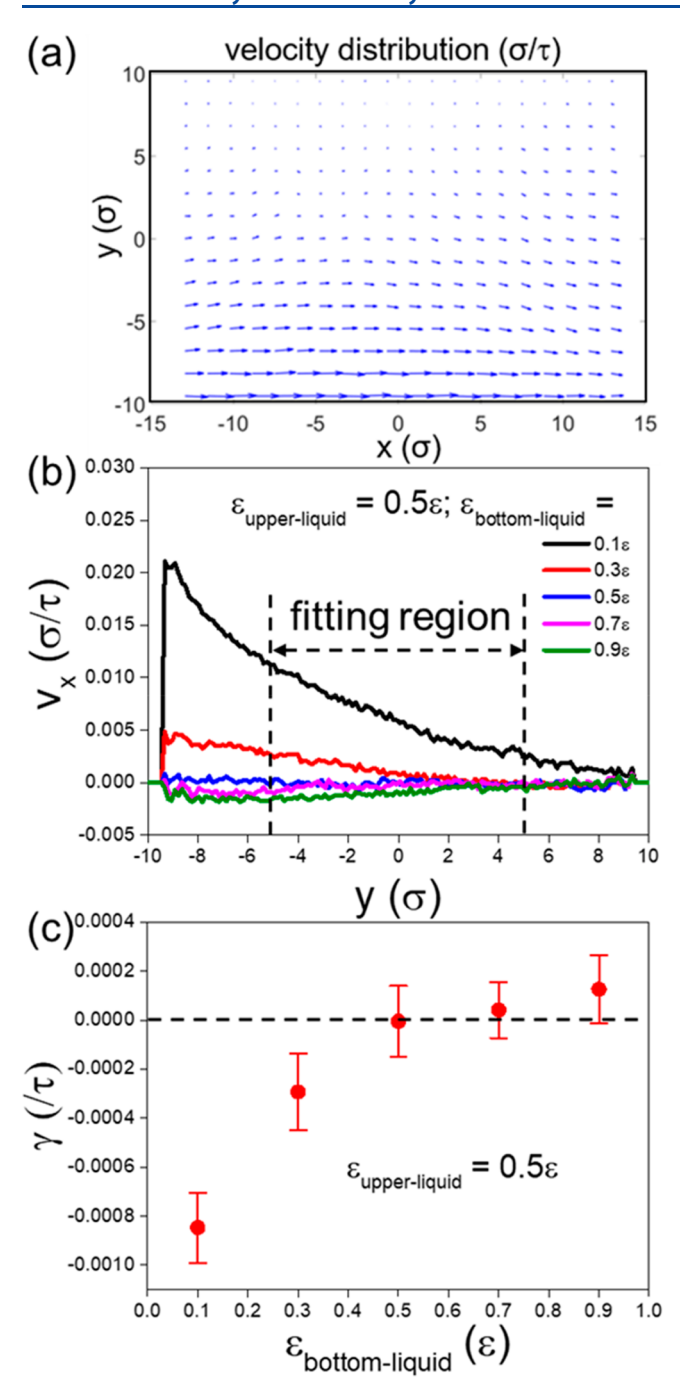


**Figure 2.** (a) Velocity field in the *x*-*y* plane inside the nanochannel for  $\varepsilon_{\text{upper-fluid}} = 0.5\varepsilon$  and  $\varepsilon_{\text{bottom-fluid}} = 0.1\varepsilon$  under the temperature difference  $\Delta T = 0.2\varepsilon/k_{\text{b}}$ . (b) Velocity profiles in the flow direction  $v_x$  inside the nanochannel for varied values of  $\varepsilon_{\text{bottom-fluid}}$  and a fixed value of  $\varepsilon_{\text{upper-fluid}} = 0.5\varepsilon$  under the temperature difference  $\Delta T = 0.2\varepsilon/k_{\text{b}}$ . (c) Shear rate *γ* as a function of  $\varepsilon_{\text{bottom-fluid}}$  for  $\varepsilon_{\text{upper-fluid}} = 0.5\varepsilon$  and  $\Delta T = 0.2\varepsilon/k_{\text{b}}$ .

 $\approx 10^8$ /s, which is significantly larger compared with the typical range in biological systems and lab experiments, i.e.,  $1-10^3$ /s.

One may argue that such giant shear rates may be ascribed to the very large temperature gradient employed in our simulation. To recognize the results from thermal noise, we employed a large temperature gradient, which may not appear in realistic experiments. However, by using a more realistic value of temperature gradient of  $\sim 0.01$  K/nm, which has been recently reported in a thermo-osmosis experiment in a

microchannel,  $^{43}$  the shear rates are still roughly estimated to be on the order of  $\sim 10^6/s$ . This indicates that our approach is sufficient to meet the real requirements of shear rates.

The mechanism of the formation of shear flows is supposed to be due to the fluid flow velocity differences near the surfaces with various wetting behaviors. As shown in Figure 2b,c, in the absence of the surface energy heterogeneity for  $\varepsilon_{\text{upper-fluid}} = \varepsilon_{\text{upper-fluid}} = 0.5\varepsilon$ , shear rates vanish. With the increased surface heterogeneity, shear rates are enhanced. Especially, the enhancement is remarkable with the presence of the hydrophobic surface.

The direction and magnitude of the fluid flow velocities near the surfaces under a temperature gradient are believed to be controlled by thermo-osmosis. To understand that, we obtain the excess surface enthalpy profiles near the bottom surfaces with various wetting behaviors, as shown in Figure 3b. The local enthalpy H(y) can be obtained from the following expression as  $^{44}$ 

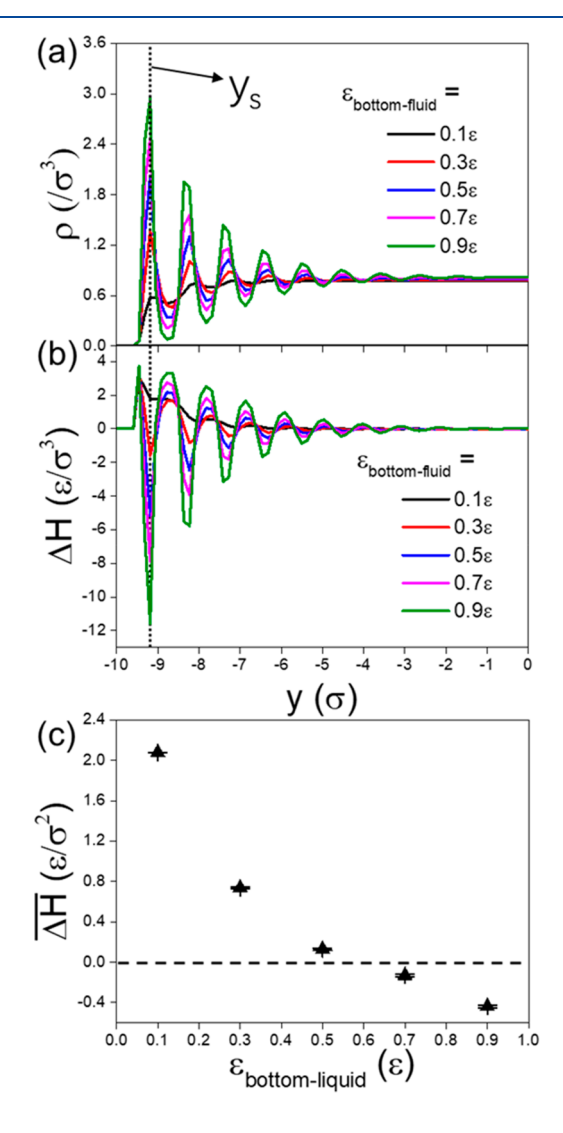


Figure 3. (a) Fluid density  $(\rho)$  and (b) excess surface enthalpy  $(\Delta H)$  profiles inside the nanochannel near the bottom surface for varied values of  $\varepsilon_{\rm bottom-fluid}$ . (c) Effective excess surface enthalpy  $(\overline{\Delta H})$  as a function of the interaction energy between the bottom surface and the fluid,  $\varepsilon_{\rm bottom-fluid}$ .

$$H(y) = \frac{\sum_{i}^{N(y)} \langle u_i + p_{i,xx} \rangle}{V(y)}$$
 (2)

where N(y) and V(y) are the number of fluid particles and the volume of the bin region at position y;  $u_i$  is the specific internal energy of particle i, including kinetic and potential energy, and  $p_{i,xx}$  is the virial expression for pressure in the x-direction. The stress tensor for each atom can be measured using the expression<sup>45</sup>

$$p_{i,ab} = mv_{i,a}v_{i,b} + \frac{1}{2} \sum_{j}^{N} \sum_{j \neq i} \left\langle \frac{r_{ij,ab}^{2}}{r_{ij}} \phi'(r_{ij}) \right\rangle$$
(3)

where a and b mean x, y, and z components; N is the total number of particles in the simulation system; m and v are the mass and velocity of particle i;  $r_{ij}$  is the distance between particles i and j, and  $\phi(r_{ij})$  is the interaction potential.

In Figure 3b, all curves of excess surface enthalpy on surfaces with different wetting behaviors show oscillations and then converge to zero at around  $6\sigma$  from the wall surfaces. Except for  $\varepsilon_{\rm bottom-fluid}=0.1\varepsilon$ , wherein the excess surface enthalpy is always positive near the wall surface, other curves significantly oscillate around zero, having both positive and negative values. In order to determine the sign of the effective excess surface enthalpy  $\overline{\Delta H}$ , which dictates the direction of thermo-osmosis, the following expression is introduced:

$$\overline{\Delta H} = \int_{y_s}^{0} \delta H(y) dy \tag{4}$$

where  $\delta H(y)$  is the excess surface enthalpy compared to the bulk, which can be estimated via  $\delta H(y) = H(y) - H(0)$ , where y is the distance to the surface of the nanochannel; y=0 is at the center of the nanochannel, and  $y=\pm 10\sigma$  is around the position of the wall surfaces. The position of the shear plane  $y_s$ , where the slip boundary condition is applied, is selected as the first peak of the fluid density profiles, as marked in Figure 3a. Figure 3c shows the effective excess surface enthalpy  $\overline{\Delta H}$  for various interaction energies between the bottom wall and the fluids  $\varepsilon_{\rm bottom-fluid}$ . For  $\varepsilon_{\rm bottom-fluid} < 0.5\varepsilon$ ,  $\overline{\Delta H} > 0$ , the fluid migrates from the high- to low-temperature region, while for  $\varepsilon_{\rm bottom-fluid} > 0.5\varepsilon$ ,  $\overline{\Delta H} < 0$ , the fluids moves from the low- to high-temperature region, as confirmed by the velocity profiles in Figure 2b.

The thermo-osmosis coefficients  $\beta_{12}$  can be deduced from the excess surface enthalpy by considering the effect of the position of the shear plane  $y_s$  and the possible slip length  $b^{46}$ 

$$\beta_{12} = -\frac{1}{\eta} \int_{y_{s}}^{0} (y - y_{s} + b) \delta H(y) dy$$
 (5)

This method has been proved efficient in electro-osmosis. An and diffusio-osmosis. Bocquet et al. related the slip length b to the interfacial friction coefficient  $\lambda^{49}$ 

$$b = \frac{\eta}{\lambda} \tag{6}$$

where  $\eta$  is the bulk viscosity, which can be estimated using a Green–Kubo relation<sup>50</sup>

$$\eta = \frac{V}{k_{\rm b}T} \int_0^t \langle p_{xy}(t) p_{xy}(0) \rangle \mathrm{d}t \tag{7}$$

where V and T are the system volume and temperature, respectively, and  $k_{\rm h}$  is the Boltzmann constant.

The interfacial friction coefficient  $\lambda$  can be evaluated from a Green–Kubo relation

$$\lambda = \frac{1}{Ak_{b}T} \int_{0}^{t} \langle F_{i}(t)F_{i}(0)\rangle dt$$
(8)

where A is the surface area of the wall contacting with fluids, and  $F_i$  is the total tangential force parallel to the wall surface. We performed another two equilibrium molecular dynamics simulations to determine the bulk viscosity  $\eta$  and the interfacial friction coefficient  $\lambda$ . The simulation details can be seen in our previous work. <sup>42</sup>

Figure 4a shows the thermo-osmosis coefficients predicted by eq 5 as a function of wall-fluid interaction energy  $\varepsilon_{\rm bottom-fluid}$ . Using typical values of  $\sigma=0.34$  nm and  $\tau=2$  ps, the moderate thermo-osmosis coefficients between  $0.5\varepsilon$  and  $0.7\varepsilon$  is on the order of  $|\beta_{12}| \approx 0.1\sigma^2/\tau \approx 10^{-9}$  m²/s, which is

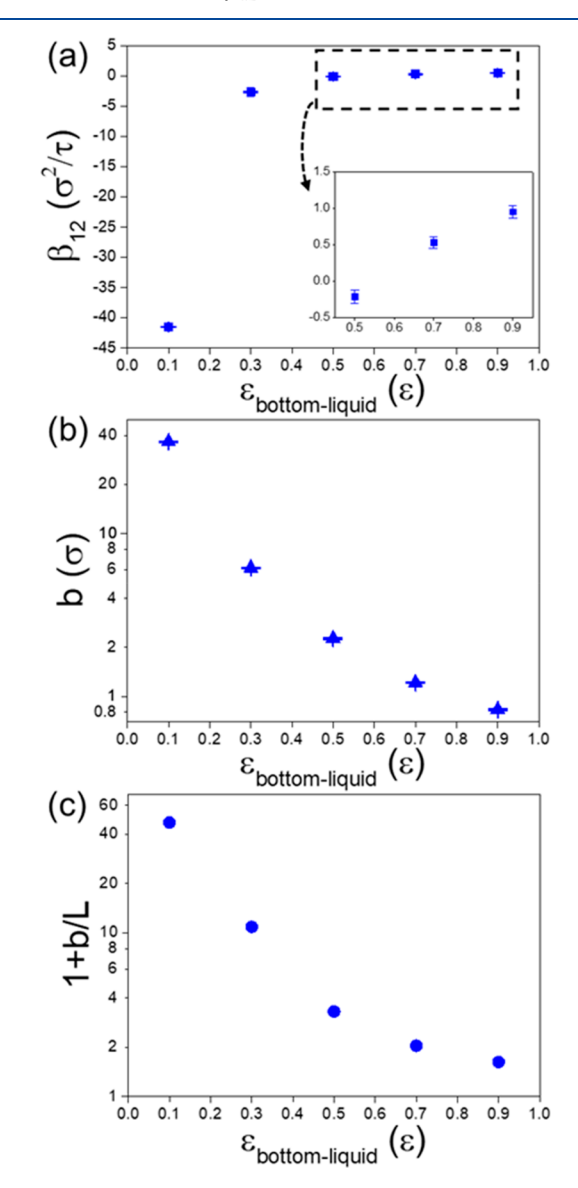


Figure 4. (a) Theoretical thermo-osmosis coefficient  $\beta_{12}$ , (b) slip length b, and (c) amplification factor 1+b/L as functions of the interaction energy between the bottom surface and the fluid,  $\varepsilon_{\text{bottom-fluid}}$ .

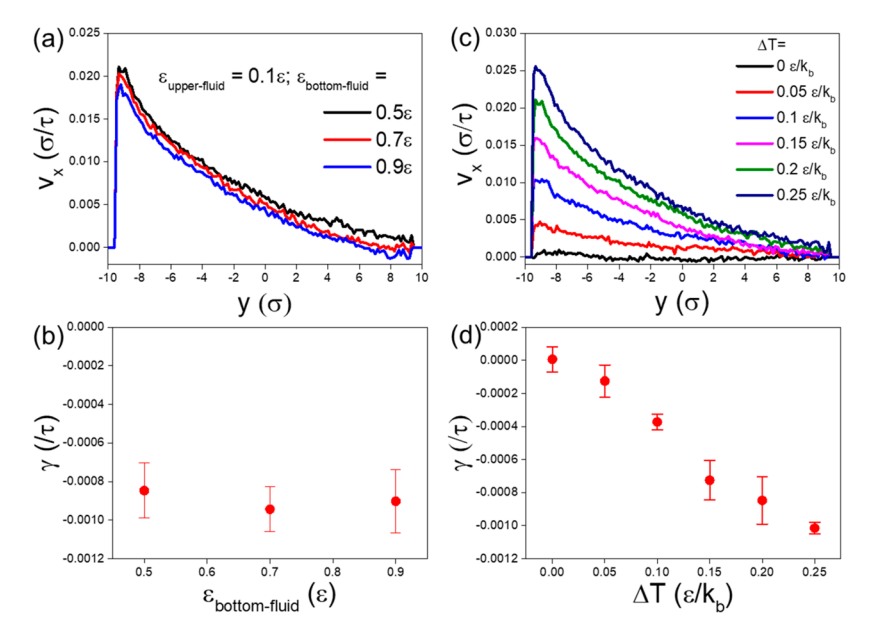


Figure 5. (a) Velocity profiles in the flow direction  $v_x$  inside the nanochannel and (b) shear rates  $\gamma$  for varied values of  $\varepsilon_{\text{bottom-fluid}}$  and a fixed value of  $\varepsilon_{\text{upper-fluid}} = 0.1\varepsilon$  under the temperature difference  $\Delta T = 0.2\varepsilon/k_b$ . (c) Velocity profiles in the flow direction  $v_x$  inside the nanochannel and (d) shear rates  $\gamma$  for  $\varepsilon_{\text{upper-fluid}} = 0.5\varepsilon$  and  $\varepsilon_{\text{bottom-fluid}} = 0.1\varepsilon$  under various temperature differences  $\Delta T$ .

comparable to the experiment value of  $10^{-10}-10^{-9}$  m²/s reported by Bregulla et al. <sup>43</sup> For  $\varepsilon_{\rm bottom-fluid} < 0.5\varepsilon$ ,  $\beta_{12} < 0$ ; for  $\varepsilon_{\rm bottom-fluid} > 0.5\varepsilon$ ,  $\beta_{12} > 0$ . This sign change also accounts for the direction change of fluid velocity, consistent with the prediction by effective surface enthalpy  $\overline{\Delta H}$ . Especially for  $\varepsilon_{\rm bottom-fluid} = 0.1\varepsilon$ , the thermo-osmosis coefficient is significant, which accounts for the much large velocity near such bottom surface and results in the highest shear rate. Our analysis shows it is mainly caused by the slip length as shown below.

To clarify the effect of slip length, eq 5 can be rewritten as 46

$$\beta_{12} = \beta_{12,\text{no-slip}} (1 + b/L)$$
 (9)

where  $\beta_{12,\text{no-slip}}$  represents the thermo-osmosis coefficients for the no-slip boundary conditions, and 1+b/L is to quantify the amplification induced by the slip length. The characteristic length L can be estimated by

$$L = \frac{\int_{y_s}^{0} (y - y_s) \delta H(y) dy}{\int_{y_s}^{0} \delta H(y) dy}$$
(10)

As the characteristic length L is very small,  $\sim 1\sigma$ , the slip length up to  $\sim 35\sigma$  for  $\varepsilon_{\rm bottom-fluid}=0.1\varepsilon$  would significantly enhance the thermo-osmosis by  $\sim 45$ -fold. This substantial enhancement, assumed to be caused by the large ratio between the slip length and the very thin interfacial layer, has also been reported particularly for thermo-osmosis<sup>46</sup> and diffusio-osmosis,  $^{51,52}$  but not for electro-osmosis for which the interfacial layer, also called the Debye layer, is generally tens of nanometers and even micrometers in thickness. Accordingly, the much larger velocity for the low values of  $\varepsilon_{\rm bottom-fluid}$  should be mainly induced by the slip length, and this would be responsible for the much larger shear rates in Figure 2b,c.

To form the shear flows, we suggested that one surface is hydrophobic and the other is hydrophilic. As shown in Figure 5b, however, if the wetting behavior of the bottom surface is fixed at very hydrophobic ( $\varepsilon_{\rm bottom-fluid}=0.1\varepsilon$ , contact angle  $\theta\approx180^{\circ}$ ), the shear rates hardly change when the wetting behavior

of the upper surface varies from moderately to very hydrophilic ( $\varepsilon_{\rm bottom\text{-}fluid}=0.9\varepsilon$ , contact angle  $\theta\approx0^{\circ}$ ). The result stems from the fact that the thermo-osmosis velocity is much larger on the very hydrophobic surface than on the hydrophilic surface, as shown in Figure 5a. Accordingly, the change of the thermo-osmosis velocity on different nonhydrophobic surfaces is insignificant and hardly alters the shear rates. The result indicates that fabrication of very hydrophobic surfaces can play a critical role in generating shear rates as large as possible, and fabrication of very hydrophilic surfaces is not essential.

It should be noted the contact angle is just a supplementary calculation to illustrate the wetting behavior controlled by the fluid-wall interaction energy and determine the rough range of the fluid-wall interaction energy. Although the contact angle of around  $180^{\circ}$  for  $\varepsilon_{\rm bottom-fluid} = 0.1\varepsilon$  is hard to achieve experimentally, the large slip length could be achieved. The maximum value of slip length is about  $37\sigma$  (~12.6 nm) in our work. Much larger experimental values of slip length even up to micrometers have been reported, as reviewed by Bocquet et al.<sup>53</sup> Therefore, much larger shear rates are expected to be achieved in real applications. It should be also noted that a simple Lennard-Jones fluid is employed in our model, which considers only the van der Waals forces but not hydrogen bonding and electrostatic forces. Our work can provide a basic theoretical framework, but further concrete investigations are needed for real applications.

Because the shear flows originate from the thermo-osmosis, temperature could provide a proper approach to controlling shear flows according to practical requirements. We use the case of  $\varepsilon_{\rm upper-fluid}=0.5\varepsilon$  and  $\varepsilon_{\rm bottom-fluid}=0.1\varepsilon$  to study the effect of temperature gradients on the shear flows. The average temperature in the middle part consisting of the nanochannel and the inside fluids is kept at  $T=0.85\varepsilon/k_{\rm b}$  by controlling the temperature in the left and right reservoirs at  $T_{\rm high}=T+\Delta t/2$  and  $T_{\rm low}=T-\Delta t/2$ , respectively. Figure 5c shows the velocity profiles in the flow direction for various temperature differences, and Figure 5d shows the shear rates as functions of the temperature difference. The thermo-osmosis velocities

on both top and bottom surfaces increase with the increased temperature gradients. Correspondingly, the shear rates also increase with the increase of the temperature gradients.

In summary, we have demonstrated a novel method of producing controllable shear flows under a temperature gradient using a heterogeneous nanochannel, one part of which is hydrophilic, while the other part is hydrophobic. We have shown that the shear flows are caused by thermo-osmosis velocity differences near the surfaces with different wetting behaviors. The thermo-osmosis velocity originates from the excess surface enthalpy and can be significantly amplified on hydrophobic surfaces by the slip length. The shear rates are sufficiently large to meet application requirements. Our findings can provide an efficient tool to achieve shear flows in experiments at micro- and nanoscale confinement. The findings also can be extended to drive micromechanical elements using torques generated by the shear flows.

#### ASSOCIATED CONTENT

## **5** Supporting Information

The Supporting Information is available free of charge at https://pubs.acs.org/doi/10.1021/acs.jpclett.1c02795.

Details of the time required to reach steady flow state, derivation of Derjaguin expression for thermo-osmosis, effect of nanochannel height on shear rates, and estimation of Reynolds number (PDF)

#### AUTHOR INFORMATION

# **Corresponding Authors**

Dengwei Jing — State Key Laboratory of Multiphase Flow in Power Engineering, Xi'an Jiaotong University, Xi'an 710049, China; Email: dwjing@mail.xjtu.edu.cn

Oleg Prezhdo — Department of Chemistry, University of Southern California, Los Angeles, California 90089, United States; orcid.org/0000-0002-5140-7500; Email: prezhdo@usc.edu

#### **Authors**

Xin Wang — State Key Laboratory of Multiphase Flow in Power Engineering, Xi'an Jiaotong University, Xi'an 710049, China

Maochang Liu — State Key Laboratory of Multiphase Flow in Power Engineering, Xi'an Jiaotong University, Xi'an 710049, China; Suzhou Academy of Xi'an Jiaotong University, Suzhou, Jiangsu 215123, China; orcid.org/0000-0002-2371-4060

Complete contact information is available at: https://pubs.acs.org/10.1021/acs.jpclett.1c02795

#### **Author Contributions**

<sup>¶</sup>X.W. and M.L. contributed equally to this work.

#### Notes

The authors declare no competing financial interest.

### ACKNOWLEDGMENTS

D.J. gratefully acknowledges the financial support of the National Natural Science Foundation of China (Grant Nos. 52025061 and 51776165) and the financial support from the Royal Society-Newton Advanced Fellowship (Grant NAF \R1\191163). O.V.P. acknowledges support of the US National Science Foundation (Grant No. CHE-1900510).

#### REFERENCES

- (1) Tung, C.-K.; Ardon, F.; Roy, A.; Koch, D. L.; Suarez, S. S.; Wu, M. Emergence of Upstream Swimming Via a Hydrodynamic Transition. *Phys. Rev. Lett.* **2015**, *114*, 108102.
- (2) Hill, J.; Kalkanci, O.; McMurry, J. L.; Koser, H. Hydrodynamic Surface Interactions Enable Escherichia Coli to Seek Efficient Routes to Swim Upstream. *Phys. Rev. Lett.* **2007**, *98*, 068101.
- (3) Schroeder, C. M.; Babcock, H. P.; Shaqfeh, E. S.; Chu, S. Observation of Polymer Conformation Hysteresis in Extensional Flow. *Science* **2003**, *301*, 1515–1519.
- (4) Si, B. R.; Patel, P.; Mangal, R. Self-Propelled Janus Colloids in Shear Flow. *Langmuir* **2020**, *36*, 11888–11898.
- (5) Du Roure, O.; Lindner, A.; Nazockdast, E. N.; Shelley, M. J. Dynamics of Flexible Fibers in Viscous Flows and Fluids. *Annu. Rev. Fluid Mech.* **2019**, *51*, 539–572.
- (6) Suematsu, N. J.; Mori, Y.; Amemiya, T.; Nakata, S. Spontaneous Mode Switching of Self-Propelled Droplet Motion Induced by a Clock Reaction in the Belousov—Zhabotinsky Medium. *J. Phys. Chem. Lett.* **2021**, *12*, 7526—7530.
- (7) Foderă, V.; Pagliara, S.; Otto, O.; Keyser, U. F.; Donald, A. M. Microfluidics Reveals a Flow-Induced Large-Scale Polymorphism of Protein Aggregates. *J. Phys. Chem. Lett.* **2012**, *3*, 2803–2807.
- (8) Ford, M. C.; Saxton, M.; Ho, P. S. Sulfur as an Acceptor to Bromine in Biomolecular Halogen Bonds. J. Phys. Chem. Lett. 2017, 8, 4246–4252.
- (9) Saikia, N.; Jha, A. N.; Deka, R. C. Dynamics of Fullerene-Mediated Heat-Driven Release of Drug Molecules from Carbon Nanotubes. *J. Phys. Chem. Lett.* **2013**, *4*, 4126–4132.
- (10) Dennis, A. M.; Delehanty, J. B.; Medintz, I. L. Emerging Physicochemical Phenomena Along with New Opportunities at the Biomolecular—Nanoparticle Interface. *J. Phys. Chem. Lett.* **2016**, 7, 2139—2150.
- (11) Sridhar, R.; Lakshminarayanan, R.; Madhaiyan, K.; Barathi, V. A.; Lim, K. H. C.; Ramakrishna, S. Electrosprayed Nanoparticles and Electrospun Nanofibers Based on Natural Materials: Applications in Tissue Regeneration, Drug Delivery and Pharmaceuticals. *Chem. Soc. Rev.* 2015, 44, 790–814.
- (12) Squires, T. M.; Quake, S. R. Microfluidics: Fluid Physics at the Nanoliter Scale. *Rev. Mod. Phys.* **2005**, *77*, 977.
- (13) Gossett, D. R.; Weaver, W. M.; Mach, A. J.; Hur, S. C.; Tse, H. T. K.; Lee, W.; Amini, H.; Di Carlo, D. Label-Free Cell Separation and Sorting in Microfluidic Systems. *Anal. Bioanal. Chem.* **2010**, 397, 3249–3267.
- (14) Nakayama, K. H.; Surya, V. N.; Gole, M.; Walker, T. W.; Yang, W.; Lai, E. S.; Ostrowski, M. A.; Fuller, G. G.; Dunn, A. R.; Huang, N. F. Nanoscale Patterning of Extracellular Matrix Alters Endothelial Function under Shear Stress. *Nano Lett.* **2016**, *16*, 410–419.
- (15) Chan, N. Y.; Chen, M.; Hao, X.-T.; Smith, T. A.; Dunstan, D. E. Polymer Compression in Shear Flow. J. Phys. Chem. Lett. 2010, 1, 1912–1916.
- (16) Huang, Z.; Chen, P.; Yang, Y.; Yan, L.-T. Shearing Janus Nanoparticles Confined in Two-Dimensional Space: Reshaped Cluster Configurations and Defined Assembling Kinetics. *J. Phys. Chem. Lett.* **2016**, *7*, 1966–1971.
- (17) Deng, Y.; Kizer, M.; Rada, M.; Sage, J.; Wang, X.; Cheon, D.-J.; Chung, A. J. Intracellular Delivery of Nanomaterials Via an Inertial Microfluidic Cell Hydroporator. *Nano Lett.* **2018**, *18*, 2705–2710.
- (18) Zheng, Y.; Bai, H.; Huang, Z.; Tian, X.; Nie, F.-Q.; Zhao, Y.; Zhai, J.; Jiang, L. Directional Water Collection on Wetted Spider Silk. *Nature* **2010**, *463*, 640–643.
- (19) Shang, L.; Fu, F.; Cheng, Y.; Yu, Y.; Wang, J.; Gu, Z.; Zhao, Y. Bioinspired Multifunctional Spindle-Knotted Microfibers from Microfluidics. *Small* **2017**, *13*, 1600286.
- (20) Cheng, H.; Meng, J.; Wu, G.; Chen, S. Hierarchical Micro-Mesoporous Carbon-Framework-Based Hybrid Nanofibres for High-Density Capacitive Energy Storage. *Angew. Chem., Int. Ed.* **2019**, *58*, 17465–17473.
- (21) Xu, T.; Ding, X.; Liang, Y.; Zhao, Y.; Chen, N.; Qu, L. Direct Spinning of Fiber Supercapacitor. *Nanoscale* **2016**, *8*, 12113–12117.

- (22) Dehnhardt, G.; Mauck, B.; Bleckmann, H. Seal Whiskers Detect Water Movements. *Nature* **1998**, 394, 235–236.
- (23) Fratzl, P.; Barth, F. G. Biomaterial Systems for Mechanosensing and Actuation. *Nature* **2009**, *462*, 442–448.
- (24) Sun, C.; Lu, W.-Q.; Liu, J.; Bai, B. Molecular Dynamics Simulation of Nanofluid's Effective Thermal Conductivity in High-Shear-Rate Couette Flow. *Int. J. Heat Mass Transfer* **2011**, *54*, 2560–2567.
- (25) Sun, C.; Bai, B.; Lu, W.-Q.; Liu, J. Shear-Rate Dependent Effective Thermal Conductivity of H2o+ Sio2 Nanofluids. *Phys. Fluids* **2013**, 25, 052002.
- (26) Harasim, M.; Wunderlich, B.; Peleg, O.; Kröger, M.; Bausch, A. R. Direct Observation of the Dynamics of Semiflexible Polymers in Shear Flow. *Phys. Rev. Lett.* **2013**, *110*, 108302.
- (27) Cappello, J.; Bechert, M.; Duprat, C.; Du Roure, O.; Gallaire, F.; Lindner, A. Transport of Flexible Fibers in Confined Microchannels. *Phys. Rev. Fluids.* **2019**, *4*, 034202.
- (28) Nagel, M.; Brun, P.; Berthet, H.; Lindner, A.; Gallaire, F.; Duprat, C. Oscillations of Confined Fibres Transported in Microchannels. *J. Fluid Mech.* **2018**, 835, 444.
- (29) Berthet, H.; Fermigier, M.; Lindner, A. Single Fiber Transport in a Confined Channel: Microfluidic Experiments and Numerical Study. *Phys. Fluids* **2013**, *25*, 103601.
- (30) Uspal, W. E.; Doyle, P. S. Scattering and Nonlinear Bound States of Hydrodynamically Coupled Particles in a Narrow Channel. *Phys. Rev. E* **2012**, *85*, 016325.
- (31) Hill, E. K.; Krebs, B.; Goodall, D. G.; Howlett, G. J.; Dunstan, D. E. Shear Flow Induces Amyloid Fibril Formation. *Biomacromolecules* **2006**, *7*, 10–13.
- (32) Liu, Y.; Chakrabarti, B.; Saintillan, D.; Lindner, A.; Du Roure, O. Morphological Transitions of Elastic Filaments in Shear Flow. *Proc. Natl. Acad. Sci. U. S. A.* **2018**, *115*, 9438–9443.
- (33) Siwy, Z.; Fuliński, A. Fabrication of a Synthetic Nanopore Ion Pump. *Phys. Rev. Lett.* **2002**, *89*, 198103.
- (34) Mo, J.; Li, C.; Li, L.; Wang, J.; Li, Z. Passive Nanofluidic Diode Using Non-Uniform Nanochannels. *Phys. Fluids* **2016**, *28*, 082005.
- (35) Li, L.; Mo, J.; Li, Z. Nanofluidic Diode for Simple Fluids without Moving Parts. *Phys. Rev. Lett.* **2015**, *115*, 134503.
- (36) Liu, C.; Li, Z. Molecular Dynamics Simulation of Composite Nanochannels as Nanopumps Driven by Symmetric Temperature Gradients. *Phys. Rev. Lett.* **2010**, *105*, 174501.
- (37) Karnik, R.; Duan, C.; Castelino, K.; Daiguji, H.; Majumdar, A. Rectification of Ionic Current in a Nanofluidic Diode. *Nano Lett.* **2007**, *7*, 547–551.
- (38) Picallo, C. B.; Gravelle, S.; Joly, L.; Charlaix, E.; Bocquet, L. Nanofluidic Osmotic Diodes: Theory and Molecular Dynamics Simulations. *Phys. Rev. Lett.* **2013**, *111*, 244501.
- (39) Nabavi, M. Steady and Unsteady Flow Analysis in Microdiffusers and Micropumps: A Critical Review. *Microfluid. Nanofluid.* **2009**, *7*, 599.
- (40) Oh, K. W.; Ahn, C. H. A Review of Microvalves. J. Micromech. Microeng. 2006, 16, R13.
- (41) Plimpton, S. Fast Parallel Algorithms for Short-Range Molecular Dynamics. *J. Comput. Phys.* **1995**, *117*, 1–19.
- (42) Wang, X.; Liu, M.; Jing, D.; Mohamad, A.; Prezhdo, O. Net Unidirectional Fluid Transport in Locally Heated Nanochannel by Thermo-Osmosis. *Nano Lett.* **2020**, *20*, 8965–8971.
- (43) Bregulla, A. P.; Würger, A.; Günther, K.; Mertig, M.; Cichos, F. Thermo-Osmotic Flow in Thin Films. *Phys. Rev. Lett.* **2016**, *116*, 188303.
- (44) Ganti, R.; Liu, Y.; Frenkel, D. Molecular Simulation of Thermo-Osmotic Slip. *Phys. Rev. Lett.* **2017**, *119*, 038002.
- (45) Hansen, J.-P.; McDonald, I. R. Theory of Simple Liquids; Elsevier, 1990.
- (46) Fu, L.; Merabia, S.; Joly, L. What Controls Thermo-Osmosis? Molecular Simulations Show the Critical Role of Interfacial Hydrodynamics. *Phys. Rev. Lett.* **2017**, *119*, 214501.

- (47) Huang, D. M.; Cottin-Bizonne, C.; Ybert, C.; Bocquet, L. Ion-Specific Anomalous Electrokinetic Effects in Hydrophobic Nanochannels. *Phys. Rev. Lett.* **2007**, *98*, 177801.
- (48) Yoshida, H.; Marbach, S.; Bocquet, L. Osmotic and Diffusio-Osmotic Flow Generation at High Solute Concentration. Ii. Molecular Dynamics Simulations. *J. Chem. Phys.* **2017**, *146*, 194702.
- (49) Bocquet, L.; Barrat, J.-L. Hydrodynamic Boundary Conditions, Correlation Functions, and Kubo Relations for Confined Fluids. *Phys. Rev. E: Stat. Phys., Plasmas, Fluids, Relat. Interdiscip. Top.* **1994**, 49, 3079
- (50) Hess, B. Determining the Shear Viscosity of Model Liquids from Molecular Dynamics Simulations. *J. Chem. Phys.* **2002**, *116*, 209–217
- (51) Ajdari, A.; Bocquet, L. Giant Amplification of Interfacially Driven Transport by Hydrodynamic Slip: Diffusio-Osmosis and Beyond. *Phys. Rev. Lett.* **2006**, *96*, 186102.
- (52) Huang, D. M.; Cottin-Bizonne, C.; Ybert, C.; Bocquet, L. Massive Amplification of Surface-Induced Transport at Superhydrophobic Surfaces. *Phys. Rev. Lett.* **2008**, *101*, 064503.
- (53) Bocquet, L.; Charlaix, E. Nanofluidics, from Bulk to Interfaces. *Chem. Soc. Rev.* **2010**, *39*, 1073–1095.